Ecological Indicators 117 (2020) 106513

Contents lists available at ScienceDirect

Ecological Indicators

journal homepage: www.elsevier.com/locate/ecolind

Assessment of UAV photogrammetric DTM-independent variables for modelling and mapping forest structural indices in mixed temperate forests

Francesca Giannetti[a,*], Nicola Puletti[b], Stefano Puliti[c], Davide Travaglini[a,*], Gherardo Chirici[a]

[a] geoLAB – Laboratory of Forest Geomatics, Department of Agriculture, Food, Environment and Forestry, Università degli Studi di Firenze, Via San Bonaventura 13, 50145 Firenze, Italy

[b] CREA - Research Centre for Forestry and Wood, Arezzo, Italy

[c] Department of National Forest Inventory, Norwegian Institute for Bioeconomy Research (NIBIO), Ås 1430, Norway

ARTICLE INFO

Keywords:
Forest inventory
Structure from motion
Drone
Airborne laser scanning
Biodiversity
Precision forestry
Forest structure
DTM-independent

ABSTRACT

In the EU 2020 biodiversity strategy, maintaining and enhancing forest biodiversity is essential. Forest managers and technicians should include biodiversity monitoring as support for sustainible forest management and conservation issues, through the adoption of forest biodiversity indices. The present study investigates the potential of a new type of Structure from Motion (SfM) photogrammetry derived variables for modelling forest structure indicies, which do not require the availability of a digital terrain model (DTM) such as those obtainable from Airborne Laser Scanning (ALS) surveys. The DTM-independent variables were calculated using raw 3D UAV photogrammetric data for modeling eight forest structure indices which are commonly used for forest biodiversity monitoring, namely: basal area (G); quadratic mean diameter (DBH_{mean}); the standard deviation of Diameter at Breast Height (DBH_{σ}); DBH Gini coefficient (Gini); the standard deviation of tree heights (H_{σ}); dominant tree height (H_{dom}); Lorey's height (H_l); and growing stock volume (V). The study included two mixed temperate forests areas with a different type of management, with one area, left unmanaged for the past 50 years while the other being actively managed. A total of 30 field sample plots were measured in the unmanaged forest, and 50 field plots were measured in the actively managed forest. The accuracy of UAV DTM-independent predictions was compared with a benchmark approach based on traditional explanatory variables calculated from ALS data. Finally, DTM-independent variables were used to produce wall-to-wall maps of the forest structure indices in the two test areas and to estimate the mean value and its uncertainty according to a model-assisted regression estimators. DTM-independent variables led to similar predictive accuracy in terms of root mean square error compared to ALS in both study areas for the eight structure indices (DTM-independent average $RMSE_{\%}$ = 20.5 and ALS average $RMSE_{\%}$ = 19.8). Moreover, we found that the model-assisted estimation, with both DTM-independet and ALS, obtained lower standar errors (SE) compared to the one obtained by model-based estimation using only field plots. Relative efficiency coefficient (RE) revealed that ALS-based estimates were, on average, more efficient (average RE ALS = 3.7) than DTM-independent, (average RE DTM-independent = 3.3). However, the RE for the DTM-independent models was consistently larger than the one from the ALS models for the DBH-related variables (i.e. G, DBH_{mean}, and DBH_{σ}) and for V. This highlights the potential of DTM-independent variables, which not only can be used virtually on any forests (i.e., no need of a DTM), but also can produce as precise estimates as those from ALS data for key forest structural variables and substantially improve the efficiency of forest inventories.

1. Introduction

New methods and tools for the integration of spatial and temporal dimensions in forest ecosystems monitoring are needed to support sustainable forest management in taking into consideration the vast array of ecosystem services provided by forests (Fotakis et al., 2012; Santopuoli et al., 2019; Shang et al., 2019; Winter et al., 2018). The protection of forest biodiversity is an increasingly important issue at European level (Arabatzis, 2010; European Environment Agency, 2012; FOREST EUROPE, 2015; Fotakis et al., 2012; Galluzzi et al., 2019; Kurttila, 2001). The European Union (2013), in the 2020 strategy for EU biodiversity, highlights the need to increase the contribution of

* Corresponding authors.
E-mail address: francesca.giannetti@unifi.it (F. Giannetti).

https://doi.org/10.1016/j.ecolind.2020.106513
Received 31 January 2019; Received in revised form 22 April 2020; Accepted 10 May 2020

forestry in maintaining and enhancing biodiversity. Moreover, it is reported that by 2020 forest management plans, or equivalent instruments, in line with sustainable forest management, need to provide "*measurable improvement in the conservation status of forest ecosystems and species and in the provision of related ecosystem services as compared to the EU 2010 Baseline*" (European Commission, 2013). As a consequence forest managers should include biodiversity monitoring in the phase of information acquisition to support forest management choices (Arabatzis, 2010; European Commission, 2013; European Environment Agency, 2012; Ozdemir, 2008; Winter et al., 2018).

In the context of precision forestry (Taylor et al., 2002), to plan and to conduct site-specific forest management, the demands for small-scale forest information have increased. Maps representing the forest environment under different points of view, for instance through multiple biodiversity indicators, are considered crucial to support forest management activities (Corona et al., 2017; Fardusi et al., 2017). For these reasons, the development of objective and robust methods to model and map biodiversity indicators is urgently needed.

Frequently, forest biodiversity is described and measured through indicators based on species compositions (Zellweger et al., 2013), or structural diversity (McElhinny et al., 2005; Mura et al., 2015). Alpha or beta biodiversity indicators based on species composition are well known and established in vegetation science and conservation biology (Noss, 1990). Forest structure indicators are related to the spatial arrangement of the different components of the forest ecosystem, such as tree heights at different canopy levels, tree spacing, and dimensioning (McElhinny et al., 2005). Forest structure is considered one of the most important indicators of forest health (Franklin and DeBell, 1988; Mura et al., 2015; Zellweger et al., 2013) and a good predictor of habitat quality for several animal species (Batisteli et al., 2018; Beedy, 1981; Bergner et al., 2015; Hanle et al., 2020; Lindberg et al., 2015; McElhinny et al., 2005). Several authors reported that maintaining and improving the complexity of forest structure is crucial to counteract the loss of biodiversity (Adhikari et al., 2020; Bagaram et al., 2018; Bottalico et al., 2017; Chirici et al., 2012; Corona et al., 2011; Immitzer et al., 2016; Kolb et al., 1994; Vihervaara et al., 2015; Winter et al., 2018; Zellweger et al., 2013). The most common structure diversity indices are based on simple information collected in plots measured in the field in the framework of forest inventories such as tree diameters at breast height (DBH) and tree heights (H) (McElhinny et al., 2005).

Three dimensional (3D) Remotely Sensed (RS) data are often used as auxiliary information to model and predict forest biophysical variables (Brosofske et al., 2014; Corona, 2010; Fotakis et al., 2012; Mura et al., 2015; Valbuena et al., 2016; van Ewijk et al., 2019), including forest biodiversity indicators (Bottalico et al., 2017; Mura et al., 2015; Valbuena et al., 2016; van Ewijk et al., 2019). Several types of variables extracted from the RS data can be used to model and predict forest biodiversity indicators. Variables describing the vertical and horizontal distribution of the trees in the canopy can be derived from 3D RS data.

Often, variables describing the distribution of trees height, are extracted from 3D point clouds such as those from Airborne Laser Scanner (ALS) (Bottalico et al., 2017; Evans et al., 2009; Lefsky et al., 2002; Lim et al., 2003; Mura et al., 2016; Teobaldelli et al., 2017; Valbuena et al., 2013; van Ewijk et al., 2019; Winter et al., 2018; Zimble et al., 2003). Lefsky et al. (2002) and Lim et al. (2003) highlighted the potential of using ALS returns to estimate canopy structure and functions, and to predict forest stands variables such as height, biomass, and volume. Zimble et al. (2003) showed that ALS-derived tree heights could be useful in the detection of differences in vertical forest structure with acceptable accuracies. Evans et al. (2009) underline how ALS pulses can be useful to develop different types of variables for a better comprehension of forest structure and spatial dynamics. Moreover, other authors have found that these ALS metrics can be used as predictors of spatial structure indices (e.g. DBH, H, Growing Stock Volume, standard deviation of DBH, standard deviation of H, Gini Coefficient, and Lorenz curve) in different forest types including boreal (Valbuena et al., 2016), Mediterranean (Bottalico et al., 2017; Teobaldelli et al., 2017), and temperate biomes (Mura et al., 2015). Niemi and Vauhkonen, (2016) and Ozdemir & Donoghue (2013) reported that the combination of traditionally ALS metrics and textural variables computed on ALS high-resolution raster grid Canopy Height Model (CHM) (i.e. pixel size 0.5 m) are useful to improve the estimation accuracy of traditional forest variables (e.g. stem volume, basal area) as well as for forest structure indicators (e.g. tree height diversity and tree DBH diversity). Moreover, Van Ewijk et al. (2019) demonstrated that the use of texture and intensity variables calculated on the basis of ALS data improved the prediction of quadratic DBH and stem density.

Variables describing the horizontal distribution of trees have also been adopted in the literature. Among these, textural variables (Haralick et al., 1973) have been used to describe the horizontal distribution of forests. Textural metrics derived from high-resolution satellite and aerial images were found to be useful for predicting forest structure indices and forest cover changes (Bruniquel-Pinel and Gastellu-Etchegorry, 1998; Gómez et al., 2012; Ozdemir and Karnieli, 2011). For example, St-Onge and Cavayas, (1995) yielded relatively accurate estimates of crown diameter, stand density, and percent cover using a MEIS-II image with a ground resolution of 36 cm. Bruniquel-Pinel and Gastellu-Etchegorry (1998) demonstrated the utility of textural metrics to predict tree position, Leaf Area Index, and crown cover from high spatial resolution airborne images acquired by RAMI pushbroom instruments. Moreover, Ozdemir and Karnieli (2011) demonstrated that Basal Area (G), Standard Deviation of DBH (DBH_σ), and DBH Gini Coefficient (Gini), can be predicted and mapped with a reasonable accuracy using the texture features extracted from the spectral bands of a WorldView-2 image. Gómez et al. (2012) found that texture variables derived from imagery captured with QuickBird-2 in a Mediterranean pine forest are also useful to map forest structural diversity indices such as DBH, H, and crown diameters.

New methods in computer vision and stereo-matching algorithms have increased the number of predictors that can be calculated from 3D photogrammetric data (Bohlin et al., 2012; Iglhaut et al., 2019; Nowak et al., 2019; Puliti et al., 2015). Nowak et al. (2019) and Iglhaut et al. (2019) in their reviews reported the complete list of works and applications developed with unmanned aerial vehicles (UAVs) and Structure from Motion (SfM) Photogrammetry to predict and to map forest structure indicators in the context of forest inventories and biodiversity monitoring.

The increasing attention to 3D photogrammetry is also due to the recent advancements in RS using lightweight UAVs equipped with digital cameras. In fact, UAV can provide at forest management scale an alternative low cost option to acquire multi-temporal RS data (Bagaram et al., 2018; Hese and Behrendt, 2017; Lisein et al., 2013; Puliti et al., 2019; Saarinen et al., 2018; Shen et al., 2019; Wallace et al., 2016; Zahawi et al., 2015). For example, Shen et al. (2019) used spectral and structural predictors derived by UAV-based multispectral and RGB photogrammetric point cloud to predict forest structural attributes such as Lorey's mean height (HL) and Growing Stock Volume. Saarinen et al. (2018) applied individual tree crown approach (ITC) and semi-individual tree crown approach (semi-ITC) in estimating plot-level biodiversity indicators with UAV-based hyperspectral imagery. They found that biodiversity indicators like the amount of deadwood and species richness were mainly underestimated with photogrammetric point clouds, while indicators of structural variability (i.e., DBH_σ and H) were the most accurately estimated biodiversity indicators with relative Root Mean Square Error (RMSE) between 24.4% and 29.3%. Giannetti et al. (2018a) developed a new set of Digital Terrain Model (DTM) independent explanatory variables to model and map traditional forest inventory variables (e.g. stem volume) from raw UAV photogrammetric data (i.e. without the input of external ALS DTM data). These variables describe both the vertical and horizontal distribution of the trees and the vegetation's spectral properties. DTM-independent variables are very promising as they enable to extend the use of UAVs beyond only

those areas where accurate DTMs are available. Puliti et al. (2020) adopted the DTM-independent approach developed by Giannetti et al. (2018a) to estimate the mean and its uncertainty for traditional forest inventory variables in a *Pinus radiata* plantation in New Zealand. Their results showed that these variables performed similarly to ALS and better than UAV laser scanning data even though there was some indication of potential bias when using DTM-independent variables for estimation purposes. Given the relevance of DTM-independent variables remains crucial to further assess their use for modelling different types of variables and in different forest types. To our knowledge, the potential of UAV photogrammetric DTM-independent explanatory variables to model and map structural complexity indices was not investigated yet.

The objective of this study was to demonstrate the feasibility of using DTM-independent variables (Giannetti et al., 2018a) from 3D UAV photogrammetric data as predictor variables for modelling and mapping, according to an area-based approach (Næsset, 2002), the following forest structure complexity indices: basal area (G; $m^2\ ha^{-1}$), quadratic mean diameter (DBH_{mean}; cm), the standard deviation of DBH (DBH_σ; cm), DBH Gini coefficient (Gini), standard deviation of H ($H_{\sigma\ h}$; m), dominant height (H_{dom}; m), Lorey's height (H_l; m), and stem volume (V; $m^3\ ha^{-1}$). The accuracy of models based on DTM-independent variables was compared with that of models based on more traditional predictors calculated on ALS data. Moreover, we produced wall-to-wall maps with both DTM-independent and ALS models to estimate mean values of forest structure indices and their uncertainty according to model-assisted regression estimators.

2. Materials and methods

2.1. Study areas

The experiment was carried out in two study areas located in central Italy, in the Apennine mountains of Tuscany Region within the province of Florence (Fig. 1).

The first study area (115 ha) is located in the State forest of Vallombrosa. At the end of the 1970s the State forest was declared Nature Reserve and management aims, which in the past were oriented to wood production, were reoriented towards multifunctionality and biodiversity conservation. As a result, during the past 40–50 years, most of the forest was undisturbed and left to natural evolution. The Reserve is included in the Special Areas of Conservation (SAC) "Vallombrosa and S. Antonio Forest" (IT5140012) under the Natura 2000 Network (Habitats Directive 92/43/EC), two priority habitats (9210* and 9220*) are included in the SAC. The study area is characterized by steep slopes (mean slope = 41%) and high altitude difference (1080–1432 m a.s.l.). The forest is dominated by pure European beech (*Fagus sylvatica* L.) stands with other isolated broadleaves (Common ash (*Fraxinus excelsior* L.), oaks (*Quercus cerris* L.), European hop-hornbeam (*Ostrya carpinifolia* Scop.), common holly (*Ilex aquifolium* L.), sycamore (*Acer pseudoplatanus*. l.) and ilex (*Ilex aquifolium* L)), silver fir (*Abies alba* M.) plantations, and other conifers plantations (*Pseudotsuga menziesii* Franco, *Pinus Nigra* J.F. Arnold, *Chamaecyparis*, Spach) (Fig. 1). The beech forests are even-aged (155–230 year) stands with simplified forest structures, which are mostly derived from coppices converted to high-forests. All the conifers plantations are even-aged. Silver fir plantations derived by the traditional management systems carried out in Vallombrosa by local monks for wood production with a traditional rotation age of 100 years. More details about the management history of Vallombrosa forest can be found in Bottalico et al. (2014). Douglas fir and Chamaecyparis are experimental plantations started in 1926 and 1922, respectively. The black pine plantations began in 1923 to replace silver fir and chestnut stands damaged by pathogens. Mixed deciduous broadleaves forests are scarcely represented in the study area and are mostly aged coppices used in the past for firewood production.

The second study area has a total area of 290 ha and is located in the District of Rincine (Florence), and it is a public property of the Tuscany region which is actively managed for timber production. The area is located at an altitude ranging between 500 and 900 m a.s.l. The forest composition is characterized by oaks (*Quercus cerris* L., *Quercus pubescens* L.) mixed whit other broadleaves (*Ostrya carpinifolia Scop*; *Carpinus betulus* L.; *Fraxinus ornus*, L.; *Prunus avium* L.; *Ulmus* spp.), European beech (*Fagus sylvatica* L.), chestnut (*Castanea Sativa* Mill.), and conifer plantations dominated by *Pinus Nigra* J.F.Arnold and *Pseudotsuga menziesii* Franco with several other non-indigenous species (*Cedrus libani*, A.Rich., *Cupressus Arizzonica*, *Chamaecyparis*, Spach) (Fig. 1). The conifer plantations are even-aged experimental trials started between 1965 and 1975 for pulpwood production. The broadleaves forests are mostly manage as coppice for firewood production. The Rincine forest management follows the criteria of Sustainable Forest Management certified by both Forest Stewardship Council (FSC) and by the Programme for the Endorsement of Forest Certification schemes (PEFC) systems. Rincine district is also a Model Forest (International Model Forest Network (IMFN), 2008). In particular, the objective of the Model Forest is to support the sustainable management of natural resources through a participatory, landscape-level approach that reflects environmental and socio-economic issues from the perspectives of local needs and global concerns (International Model Forest Network (IMFN), 2008).

In the two study areas, five of the 14 European Forest Types (Barbati et al., 2014; Giannetti et al., 2017) are represented.

2.2. Field data and computation of forest structure indices

In each study area, a local field-based forest inventory was carried out (Fig. 1). In Vallombrosa field measurements were conducted in a total of 30 circular fixed-area sample plots of 13 m radius (each plot covers 530 m^2). Fieldwork was carried out in June 2015. Field plots were selected using a tessellation stratified sampling scheme (Barabesi and Franceschi, 2011) based on an hexagonal grid with hexagons of 1 ha.

In Rincine the field measurements were carried out in 50 squared fixed-area plots of an area of 530 m^2. Fieldwork was carried out between June and September 2016. Field plots were selected using the one-per-stratum stratified sampling scheme (Barabesi et al., 2012; Fattorini et al., 2016) based on a 23 × 23 m grid. The study area was partitioned into 50 strata (i.e., polygons based on equal-size strata obtained by means of clusters) and one grid cell of 23 × 23 in each stratum was selected randomly as field plot to measure.

In both study areas, the coordinates of plot centres were recorded using Global Navigation Satellite Systems (GNSS) Trimble Geo 7x dual-frequency receiver, observing the pseudorange of both GPS and GLONASS. The recorded GNSS positions were post-processed with correction from a base station into a sub-meter precision. In each plot, the DBH and height of all trees (H) with a DBH ≥ 2.5 cm were registered using a caliper and a Haglof Vertex IV device.

Field data were used to calculate a set of eight structural complexity indices based on tree DBH and height. The indices considered in this work were selected after a literature review of possible biodiversity drivers (Bottalico et al., 2017; McElhinny et al., 2005; Meng et al., 2016; Mura et al., 2015; Ozdemir and Karnieli, 2011; Valbuena et al., 2016; Ziegler, 2000). In the selection, we also considered data which are routinely acquired during National Forest Inventories. In particular, we calculated the following: four DBH related indices (G, DBH_{mean}, $_{Gini}$); one tree height-related index (H_σ) and three indices that combine DBH and H (H_l, H_{dom}, V). In the next paragraphs, the indices chosen in this study are briefly presented based on the literature review. Table 1 summarizes the mean estimates (μ_i) and the standard error (SE) of the indices for the two study areas based on design-based estimators.

Basal area (G) is a forest inventory variable describing the amount of an area (m^2) occupied by tree stems at breast height (i.e., 1.3 m above ground). G is directly related to growing stock volume and

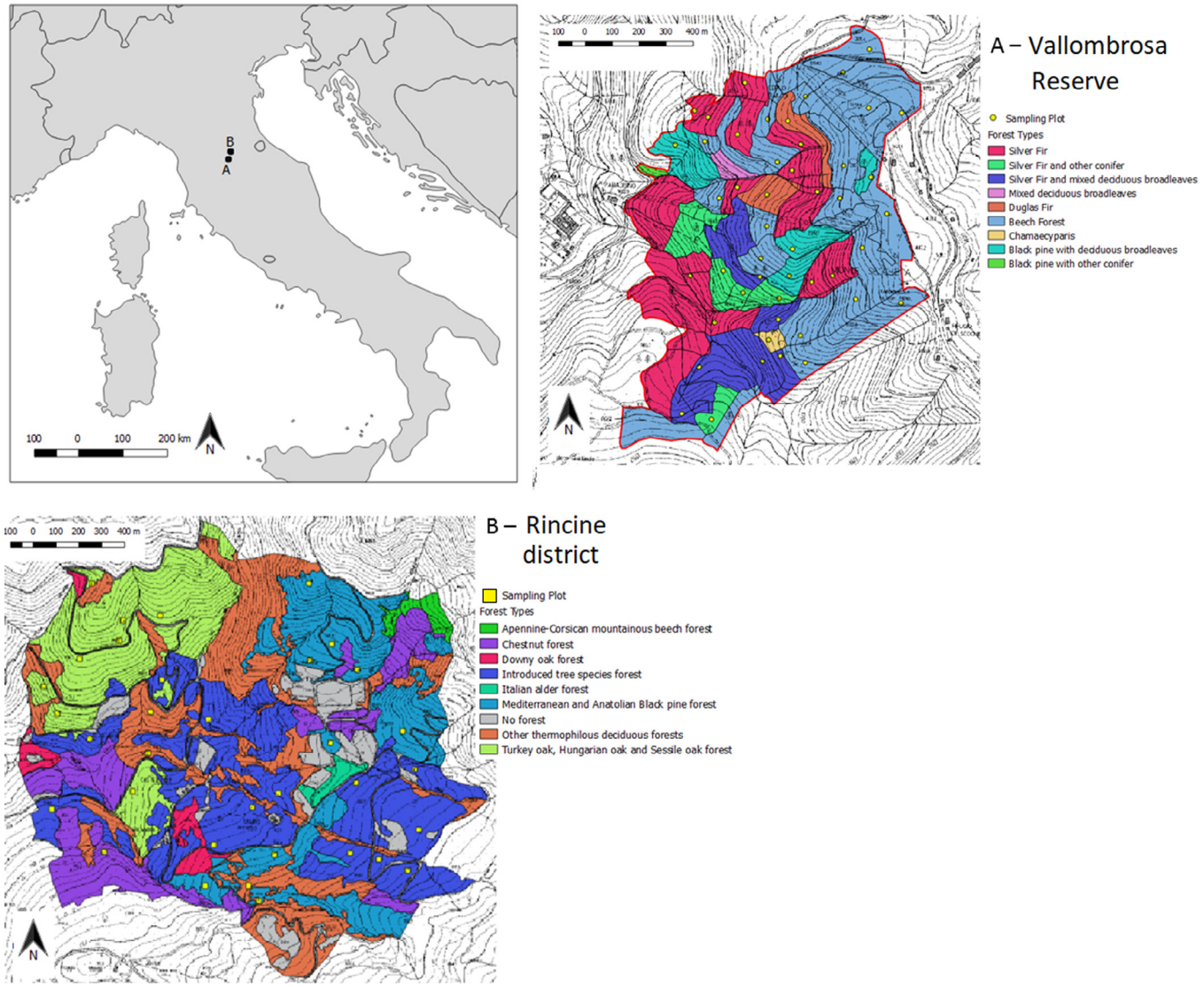

Fig. 1. Study areas with forest types and location of the field plots.

Table 1
Forest structural indices summary of design-based estimates of mean-value (μ_i) and Standard Error (SE) (Fattorini et al., 2016).

Structural index and Forest biophysical proprieties	Study area	μ_i	SE
G (m^2ha^{-1})	Vallombrosa	59.5	4.21
	Rincine	48.41	2.35
DBH_{mean} (cm)	Vallombrosa	27.6	0.02
	Rincine	27.20	1.34
DBH_σ (cm)	Vallombrosa	12.6	1.17
	Rincine	7.51	0.39
Gini (0–1)	Vallombrosa	0.46	0.17
	Rincine	0.32	0.20
H_{dom} (m)	Vallombrosa	29.4	1.57
	Rincine	23.7	1.01
H_l (m)	Vallombrosa	24.5	1.52
	Rincine	21.3	1.03
H_σ (m)	Vallombrosa	7.1	0.81
	Rincine	3.7	0.19
V (m^3ha^{-1})	Vallombrosa	624.3	42.31
	Rincine	492.9	36.40

biomass which are important variables supporting traditional forest management approaches oriented to a sustainable wood production as well as for biodiversity conservations purposes (McElhinny et al., 2005). Quadratic mean diameter (DBH_{mean}) is considered an important indicator to describe successional stages and for assessing the type of forest management and the level of naturalness of forest habitats (McElhinny et al., 2005; Uuttera et al., 1998; Ziegler, 2000). Generally, the DBH_{mean} is related to forest stand age (McElhinny et al., 2005; Ziegler, 2000). DBH_{mean} (expressed in cm) is calculated as:

$$DBH_{mean} = \sqrt{\frac{4G}{\pi n}} \quad (1)$$

where G is the total basal area (expressed in cm^2) and n is the number of trees in the plot. The standard deviation of DBH (DBH_σ) is a measure of the variability in tree size. It is considered an important indicator of micro-habitat diversity in forest stands (McElhinny et al., 2005; Mura et al., 2015; Ozdemir and Karnieli, 2011). Generally, the high degree of biodiversity is associated to high variation in stem diameters that is related to the presence of different successional stages in a given forest stand (Bradshaw and Lindén, 1997; Esseen et al., 1992). DBH_σ is calculated as:

$$DBH_\sigma = \sqrt{\frac{\sum_{i=1}^{n} (DBH_i - \overline{DBH})^2}{n-1}} \quad (2)$$

where i is the tree index, n is the number of trees in the plot, $\overline{DBH}$ is the mean plot-level diameter, and DBH_i is the diameter of the of i-th tree.

Gini coefficient (Gini) is also used for measuring tree size diversity in a forest stand (Lexerød and Eid, 2006; Valbuena et al., 2016). Theoretically, the minimum value of this coefficient is zero when all trees have equal size, while the maximum value is 1 when all trees except one have a value of zero (Meng et al., 2016; Ozdemir and Karnieli, 2011; Valbuena et al., 2016). The index describes tree size inequality for each field plot (Valbuena et al., 2016). Gini coefficient is calculated as:

$$\text{Gini} = \frac{\sum_{t=1}^{n}(2t - n - 1)G_t}{\sum_{t=1}^{n} G_t(n-1)} \quad (3)$$

where G_t is the basal area for tree in rank t (m^2ha^{-1}) and t is the rank of a tree in order from 1,…., n (Meng et al., 2016).

The standard deviation of H (H_σ), describes the variation of the trees along with the vertical stratum. Large variations in tree height are, usually, linked with a variety of tree ages and species in a stand, and can be used as an indicator of micro-habitats diversity for wildlife (Bottalico et al., 2017; McElhinny et al., 2005; Mura et al., 2015; Zenner, 2005). H_σ is calculated as:

$$H_\sigma = \sqrt{\frac{\sum_{i=1}^{n}(H_i - \overline{H})^2}{n-1}} \quad (4)$$

where i is the tree index, n is the number of trees in the plot and $\overline{H}$ is mean plot-level height and H_i is the height of the *i-th* tree.

The dominant height (H_{dom}) is an indicator of forest site productivity (Skovsgaard and Vanclay, 2008) and, at least in Italy, it is calculated as the mean height of the 100 largest trees in terms of DBH per hectares. The Lorey's height (H_l) weights the contribution of trees to the stand height by their basal area. Thus, Lorey's mean height is calculated as:

$$H_l = \frac{\sum_{i=1}^{n} G_i * H_i}{G} \quad (5)$$

where i-th is the tree index, G is the total basal area in the plot and G_i is the basal area of the i-th tree in the plot, and H_i is the height of the i-th tree in the plot. The plot-level growing stock volume (V) was calculated based on the equations developed by Tabacchi et al. (2011) in the framework of the 2nd Italian National Forest Inventory based on tree DBH and height.

2.3. UAV photogrammetric data and computation of DTM-independent predictors

A SenseFly eBee Ag fixed-wing UAV equipped with a SONY WX 18 MP RGB camera was used for image acquisition. The UAV flew over Vallombrosa in June 2015 and over Rincine in July 2016. Both flights were performed under leaf-on conditions. In each area, UAV acquisition was completed in one working day. Before UAV acquisitions, 12 ground control points (GCPs) were placed on the ground in each study area. We used 50 × 50 cm targets with a black and white checkerboard pattern to ensure the largest contrast in the images. The targets were fixed to the ground in open areas, and their coordinates were recorded with a Trimble Geo 7X receiver (Trimble, 2017); data collection lasted for approximately 15 min for each target with a 2-sec logging rate. The recorded coordinates were post-processed with correction data from the nearest ground base station using Pathfinder software. In the two study areas, the post-processed GCP coordinates revealed standard deviations for northing, easting, and height of 0.7 cm, 0.5 cm, and 1.4 cm, respectively.

The flight parameters were the same in the two study areas: flight altitude of 145 m above ground, and flight lines oriented parallel to the slope with an overlap of 85% longitudinal and 75% lateral. The flight lines parallel to the slope, and the artificial intelligence of UAV, allow the SenseFly eBee Ag fixed-wing UAV to change the height of the flight based on a DTM. This flight pattern allows maintaining a constant ground sampling distance (GSD). The total flight time was 69 min in Vallombrosa (169 ha, 1.6 ha/minute) divided into two flights, and 82 min in Rincine (290 ha, 3.5 ha/minute) divided into four flights. Flight lines spacing was 40 m and the distance between two consecutive photos was 35.7 m. The focal length of the camera was set to 4 mm and the ISO sensibility was 100 with a shutter speed of 1/2000 sec. A total of 228 images were acquired in Vallombrosa and 506 in Rincine with a field of view of 200 × 150 m. After visual inspection, the quality of the images acquired in the two study areas was considered satisfactory, without any problem related to light, atmospheric conditions, saturation, or blurriness because we flew around noon with uniform sunny condition.

Three-dimensional data were extracted from the UAV images using the Agisoft PhotoScan Pro software (Agisoft LLC, 2017). This software uses a combination of SfM and stereo-matching algorithms for image alignment and multi-view stereo reconstruction and fully automates the photogrammetric workflow. As a result 3D and 2D data can be exported as georeferenced points cloud, digital surface models (DSM) and orthophotos (Agisoft LLC, 2017). This software has been already used for forest applications (Bagaram et al., 2018; Giannetti et al., 2018b; Kachamba et al., 2016; Marra et al., 2018; Puliti et al., 2019, 2015). In the two study areas, the UAV images were processed as follows: (a) image alignment; (b) mesh building; (c) guided marker positioning and optimization of camera alignment (georeferencing of created scene), (d) dense cloud generation and (e) raster grid DSM generation with a ground resolution of 0.5 m × 0.5 m. We refer to Puliti et al. (2015) for a detailed description of processing parameters used in Agisoft Photoscan and for a detailed description of parameters associated with 3D UAV photogrammetric point-cloud generation. From the SfM photogrammetric workflow, we obtained point clouds having a density of 44.25 points m^{-2} in Vallombrosa and of 48.36 points m^{-2} in Rincine, raster grid DSM with a GSD of 0.5 m and orthomosaic with a GSD of 0.10 m in both study areas.

Based on the derived photogrammetric data, DTM-independent predictors were calculated as reported by Giannetti et al. (2018a) based on the non-normalized UAV photogrammetric point cloud and the raster grid DSM for each one of the field plots available in the two study areas clipping the point clouds and DSM by a shape representing the perimeter of the plot (e.g. a 13 m radius circle in Vallombrosa, and a 23 m side square in Rincine). Furthermore, the same variables were calculated for all grid cells of dimensions 23 m × 23 m tessellating the entire study areas to produce wall-to-wall maps of the eight structural indices. The size of the cells mimics the area of the field plots (i.e. 530 m^2).

A total of 163 DTM-independent variables were computed. In details, 148 were point cloud variables and 15 were DSM variables. The point cloud variables were computed based on *z*, *z standard*, *intensity*, *RGB* value and combined *z* and *intensity* (Giannetti et al., 2018a). The DSM variables were calculated based on average and standard deviation statistics of Grey-level co-occurrence matrix textural of mean, variance, homogeneity, contrast, dissimilarity, entropy and second moment (Haralick et al., 1973). In addition, from DSM also the number of local maxima was extracted with a search window of 3 × 3 pixel, or 1.5 × 1.5 m. A detailed description of the DTM-independent variables used in the current study can be found in Giannetti et al. (2018) and in Annex 1. The point cloud DTM-independent variables were computed using the R-CRAN package lidR (Roussel, 2020), while the DSM DTM-independent variables were computed using lidR (Roussel, 2020) and GLCM package in R (Zvoleff, 2015).

2.4. ALS data and computation of ALS predictors

In the two study areas, the ALS survey was carried out in May 2015 under leaf-on condition using a Eurocopter AS350 B3 equipped with a LiDAR RIEGL LMS-Q680i sensor. The flight height was 1000 m above ground level. Full-waveform LiDAR data were registered and discretized to a point density of 10 points m^{-2}. Standard procedures for

Table 2
ALS predictor variables.

DTM dependent metrics	Descriptive feature
Tot	Total Number of points
Min	Minimum
Max	Maximum
Avg	Average
Range	Range
Sd	Standard deviation
Var	Variance
Cv	Coefficient of variation
Iq	Interquantile distance
Sk	Skewness (Davies and Goldsmith, 1984; McGaughey, 2014)
Ku	Kurtosis (Davies and Goldsmith, 1984; McGaughey, 2014)
Aad	Average absolute deviation (McGaughey, 2014)
p1, p2, …, p95, p100	percentile of 10, 20, 30, 50, 60, 70, 80, 90, 95, 100 h distribution
p99/p25	Ratio of percentiles
p99/p50	Ratio of percentiles
p99/p75	Ratio of percentiles
d1, d2,…,d9,d10	proportion of points above the 1st,…,10th fraction to the total number of points (cutoff = 1.30)

pre-processing ALS data (e.g. outliers and noise removal, classification of ground/non-ground, and computation of height on the ground) were carried out with the LAStools software (Isenburg, 2017) in order to obtain ALS normalized point clouds. More details on the ALS data can be found in (Chirici et al., 2018).

A total of 32 predictors were calculated from the DTM normalized ALS data. These variables included typically used predictors for forest biophysical variables and included three types of predictors: statistical (McGaughey, 2014), height, and density (Næsset, 2004). The variables were computed using the R-CRAN package lidR (Roussel, 2020). A summary of ALS explanatory variables is provided in Table 2. The ALS explanatory variables were calculated as done for DTM-independent, for each one of the field plots available in the two study areas. Furthermore, the same variables were calculated for all grid cells of dimensions 23 m × 23 m tessellating the entire study areas to produce wall-to-wall maps of the eight structural indices.

2.5. Regression models

Multiple linear regression models were used fitting each forest structure indices, derived by field data, as response variables and using either the DTM-independent or the ALS explanatory variables as predictors.

The predictors were selected initially by carrying out a correlation analyses between the metrics to check for the mutually correlated variables using Person's product moment correlation (r) matrix. When two metrics have $r > 0.85$, only the one that was less correlated with other metrics was used in the models as independent variables. The best combination of explanatory variables was then selected using a subset regression procedure using a branch-and-bound algorithm (Clausen and Perregaard, 1999) implemented in the R-cran package *leaps* (Lumley, 2017). The algorithm was addressed to optimize the *Adjusted* R^2 (*Adj.* R^2) for each possible predictors combination. The algorithm was set to find at least five explanatory variables that maximized the *Adj.* R^2, searching for one-variable model, two-variables model until five-variables models. To select the best combination of predictors and to avoid overfitting, for each of the combinations selected by the branch-and-bound algorithm (one-variable, two variables until five variables models) we performed additional tests: (1) the *hypothesis test* (Piñeiro et al., 2008) and (2) the analysis of the *degree of overfitting to the sample* (Valbuena et al., 2017). The *hypothesis test* allows to assess the residual distribution analytically without the visual interpretation of the scatterplot observed vs. predicted (Piñeiro et al., 2008; Valbuena et al., 2017). Through such test, we assessed whether observed and predicted values follow the line 1:1 analyzing the intercept (α), and the slope (β) of the linear regression model between observed and predicted values:

$$y_i = \alpha + \beta \hat{y}_i \quad (6)$$

where y_i are the observed values and $\hat{y}_i$ are the predicted values derived by cross-validation using the leave-one-out procedure (LOO). The LOO was carried out by leaving out each *i*th plot iteratively, the model was then fitted using the remaining plots, applied to the *i*th observation, and the LOO residual calculated as the difference between the predicted values ($\hat{y}_i$) and the observed values (y_i). The *hypothesis test* is proven by not rejecting the null hypothesis that $\beta = 0$ and $\alpha = 1$ for

$$\hat{y}_i - y_i = \alpha + \beta \hat{y}_i \quad (7)$$

The analysis of the *degree of overfitting to the sample* was performed using a replication method comparing cross-validation results against model residual analyzing the sums of squares ratio (SSR) obtained by comparison of the same measure acquired by model fit against cross-validation (Valbuena et al., 2017). The SSR is a ratio of increase in unexpected variance and was employed to adjust the inflation of unexplained variance in the cross-validation with a limit of 10%.

The SSR was calculated as:

$$SSR = \frac{\sqrt{SS^{cv}}}{\sqrt{SS^{fit}}} \quad (8)$$

where SS^{cv} is the square root of the sum of squares attained in the cross-validation and SS^{fit} is the sum of squares of the model residuals (***j***), i.e. the value fitted without cross-validation, and are calculated as:

$$SS^{cv} = \sum_{i=1}^{n} (\hat{y}_i - y_i)^2 \quad (9)$$

$$SS^{fit} = \sum_{j=1}^{n} (\hat{y}_j - y_j)^2 \quad (10)$$

where $\hat{y}_j$ are the non cross-validated predictions and y_j are the observed values.

Moreover, for each of the models we evaluated the predictive accuracy at plot level using the LOO cross-validation procedure using *Adj.* R^2, RMSE, relative RMSE ($RMSE_{\%}$), mean difference (*MD*) and relative mean difference ($MD_{\%}$) because these parameters are the most common accuracy values used in previous studies. The accuracy parameters were calculated as:

$$MD = \frac{\sum_{i=1}^{n} (\hat{y}_i - y_i)}{n} \quad (11)$$

$$RMSE = \sqrt{\frac{\sum_{i=1}^{n} (\hat{y}_i - y_i)^2}{n}} \quad (12)$$

where ***n*** is the number of plots. $RMSE_{\%}$ was calculated as the percentage of *RMSE* on the average observed value of the variable measured in the field.

In the end, among the models that respect the $SSR < 1.1$. (i.e. means that the level of divergence of 10% is acceptable) and the hypothesis test we chose the ones that produced the higher *Adj.* R^2 and the lowest values of *RMSE*, *MD*, $RMSE_{\%}$, and $MD_{\%}$.

2.6. Mapping and estimation

The DTM-independent models and ALS models, developed in Section 2.5 were then applied to every 23 × 23 cells to produce a map for each one of the selected diversity indices in the two study areas.

Moreover, we estimated the mean and variance for all the structure indices considered for the two areas using the model-assisted regression (GREG) (Särndal et al., 2003) as done by Bottalico et al. (2017), Mura

et al. (2015) and Chirici et al. (2020).

The map-based estimate of the structure indices in one area was:

$$\hat{\mu}_{\text{map}} = \frac{1}{\text{N}} \sum_{\text{j=1}}^{\text{N}} \hat{\text{y}}_{\text{i}} \tag{13}$$

where N is the total number of 23 × 23 m forested population units in the study area and $\hat{y}_i$ is the model prediction for the *i-th* population unit of the index. The map estimate was then adjusted for systematic errors using a bias estimate calculated as:

$$\hat{\text{Bias}}(\hat{\mu}_{\text{map}}) = \frac{1}{\text{n}} \sum_{\text{i=1}}^{\text{n}} (\hat{\text{y}}_{\text{i}} - \text{y}_{\text{i}}) \tag{14}$$

where n is the sample size, $\hat{y}_i$ is the model prediction for the *i-th* sample plot and y_i is the observed value for the *i-th* plot. The GREG estimate is the map estimate with the estimated bias subtracted

$$\hat{\mu}_{\text{GREG}} = \hat{\mu}_{\text{map}} - \hat{\text{Bias}}(\hat{\mu}_{\text{map}}) \tag{15}$$

while the standard error (SE) of $\hat{\mu}_{GREG}$ is

$$\text{SE}(\hat{\mu}_{\text{GREG}}) = \sqrt{\hat{\text{Var}}(\hat{\mu}_{\text{GREG}})} = \sqrt{\frac{1}{\text{n(n-1)}} \sum_{\text{i=1}}^{\text{n}} (\text{e}_{\text{i}} - \bar{\text{e}})^2} \tag{16}$$

where

$$e_i = (\hat{y}_i - y_i) \text{ and } \bar{e} = \frac{1}{n} \sum_{i=1}^{n} e_i \tag{17}$$

In addition, to assess the efficiency of the model-assisted estimator, we compared it with the original design-based estimates produced by the field plot measures and its relative efficiency coefficient (RE) calculated as:

$$\text{RE} = \frac{\widehat{\text{Var}}(\mu_{\text{i}})}{\widehat{\text{Var}}(\mu_{\text{GREG}})} \tag{18}$$

Because RE coefficient is the ratio between the variances of $\widehat{Var}(\mu_i)$ and $\widehat{Var}(\mu_{GREG})$ (Moser et al., 2017), RE can be interpreted as the factor by which the original sample size would have to be increased to achieve the same precision as that obtained using the remotely sensed auxiliary data. The $\widehat{Var}(\mu_i)$ was calculated based on field data and the sampling design as reported in Fattorini et al. (2016) (Table 1).

3. Results

3.1. Regression models

Individual models were developed for each of the different set of predictors (UAV DTM-independent vs. ALS), for each dependent variable (i.e. the eight indices G, DBH_{mean}, DBH_{σ}, Gini, H_{σ}, H_{dom}, H_l and V) and for each of the study areas (i.e. Vallombrosa and Rincine). Using the SSR (i.e. SSR < 1.1) in conjunction with the *hypothesis test*, we found that the number of predictor entered in the models ranged between 1 and 4 for both DTM-independent (Table 3) and ALS models (Table 4). However, the models that used DTM-independent have in general, more predictors compared to the ones with ALS (Tables 3 and 4).

In Vallombrosa the DTM-independent variables resulted in consistently larger *Adj.* R^2 for G, DBH_{mean}, Gini, and H_{σ}, while ALS variables had higher *Adj.* R^2 for H_l, while comparable results between the two set of predictors were observed for V, H_{dom}, and DBH_{σ} (Tables 3 and 4). In Rincine, among the two sets of variables, DTM-independent variables produced more accurate results with larger *Adj.* R^2 for DBH_{σ} while ALS resulted in larger *Adj.* R^2 for G, H_{dom}, and H_l. In Rincine comparable results between the two set of variables were observed for Gini, H_{σ}, and V (Tables 3 and 4).

The LOO of the selected models revealed that the differences in predictive accuracy in terms of $RMSE_{\%}$ between DTM-independent and ALS models in Vallombrosa ranged between −4.65% and 3.79% while in Rincine ranged between −3.51% and 7.02% (Fig. 2). In all the selected models MD values were relatively small, never higher than 1.3% of the mean reference value measured in the field and the two-side *t-test* never revealed MD statistically significant values (*p-values* ≥ 0.82).

The analysis of the residuals revealed no violation of the assumptions of linearity, normality of the residuals, homoscedasticity, and independence for any of the models. The NCV test, the Kolmogorov Smirnov and the Durbin-Watson tests always resulted in *p-values* > 0.05. The assumptions are confirmed, also, by hypothesis test and SSR analysis (Fig. 3).

3.2. Mapping and area-wide estimation

To give an example of the possible application of DTM-independent variables to produce maps to support forest management and biodiversity monitoring, we applied the models from Tables 3 and 4 to create maps of the eight studied structure indices in the two study areas (Fig. 4). We then estimated the mean ($\hat{\mu}_{GREG}$) and the SE according to the GREG estimator for all the mapped indices derived by DTM-independent models and ALS models in both study areas (see Table 5). Moreover, we used the RE to assess the increase in precision when using remotely sensed data (i.e., model-assisted) rather than using a design-based estimate (Table 5) based on field plot data alone (Table 1). We found comparable results between the $\hat{\mu}_{GREG}$ and $SE(\hat{\mu}_{GREG})$ between model-assisted estimates that use DTM-independent models and the ones that use ALS models (Table 5). Moreover, the RE revealed that model-assisted estimates, with DTM-independent and ALS models, were more efficient compared to the ones obtained with design-based estimates (Tables 1 and 5). The RE coefficient ranged between 1.0 and 6.43 (average RE = 3.3) for DTM-independent and between 1.0 and 11.7 (average RE = 3.7) for ALS. The RE for the estimates based on the DTM-independent models was consistently larger than the one from the ALS models for the DBH-related variable (i.e. G, DBH_{mean}, and DBH_{σ}) and for V. On the other hand, the RE for height-related variables was always the largest for estimates based on ALS data. While for the Gini coefficient the RE was similar for the two study areas and larger for Rincine compared to Vallombrosa.

4. Discussion

In this study, we assessed the use of DTM-independent predictors (Giannetti et al., 2018a) calculated from 3D UAV photogrammetric data to model, to map and to derived model-based estimates of the main value and its uncertainty of eight forest structure complexity indices (*G*, DBH_{mean}, DBH_{σ}, Gini, H_{σ}, H_{dom} H_l, and V). In order to assess the relative validity of DTM-independent predictors we constrasted the results against a traditional set of predictors (i.e. ALS) and we assessed them across two different mixed temperate forests characterized by different types of management systems, i.e. the Vallombrosa forest, which in the last 40–50 years was mainly left to a natural evolution, and the Forest district of Rincine, that is actively managed with a sustainable forest management approach.

The current discussion is focused on three main aspects: (i) comparing the accuracy derived by DTM-independent regression models in modelling forest structure indices across the two forests in relation to the benchmark (i.e. ALS regression models), and the results obtained by previous research using different types of predictors; (ii) evaluate the accuracy of estimates derived using a model assisted estimator, and (iii) discuss the utility of maps in producing an inference.

DTM-independent models produced comparable results between the two studied areas in terms of *Adj.* R^2 (i.e. Vallombrosa: 0.40 ≤ *Adj.* R^2 ≤ 0.79; Rincine: 0.38 ≤ *Adj.* R^2 ≤ 0.78), but in terms of $RMSEs_{\%}$ slightly more accurate results were observed in Vallombrosa (12.81% ≤ $RMSE_{\%}$ ≤ 23.29%) compared to those retrieved in Rincine

Table 3
Variables selections and models accuracies, in terms of RMSE, $RMSE_{\%}$, Adj.R^2, SRR and Hypothesis test for the multiple regression models using the UAV DTM-independent variables as predictors (α = intercept slope of observed vs predicted regression; β = slope of observed vs prediction regression; * level of significance for rejection [*not significant < 0.001]).

Structural index	Study Area	DTM-independent variables[a]	RMSE	$RMSE_{\%}$	Adj. R^2	SSR	HTα	HTβ
G [m^2ha^{-1}]	Vallombrosa	*zsd + i_4q_d10 + num_max*	7.5	12.81	0.76	0.98	1.32*	0.86*
	Rincine	*AAD_B + P99P75*	12.9	26.72	0.40	0.99	1.27*	0.85*
DBH_{mean}[cm]	Vallombrosa	*d10 + AVG_homogeneity + AVG_mean + num_max*	4.2	16.07	0.64	0.99	2.10*	0.91*
	Rincine	*I_2q_d5 + I_1q_p2*	5.3	19.77	0.71	1.09	−2.23*	0.94*
DBH_{σ}[cm]	Vallombrosa	*z_st_p10 + I_2q_p100 + SD_entropy + AVG_homogeneity*	2.8	23.31	0.62	0.93	2.14*	0.89*
	Rincine	*entropy_B + SD_dissimilarity + SD_homogeneity + AVG_dissimilarity*	1.7	22.41	0.50	0.87	2.45*	0.91*
Gini[0,1]	Vallombrosa	*I_2q_d10 + AVG_contrast + i_4_p75_p25 + i_3_p75_p25 + i_1_p75_p25*	0.09	19.14	0.58	0.92	1.25*	0.94*
	Rincine	*VCI_R + mean_G + SD_homogeneity + d8*	0.07	23.36	0.65	0.98	1.34*	0.91*
H_{dom}[m]	Vallombrosa	*I_2q_d10 + AVG_homogeneity + i_d2 + i_mean*	2.4	33.69	0.41	1.05	−1.34*	0.93*
	Rincine	*AAD + mean_R + SD_mean + d7 + d3*	1.0	29.00	0.38	0.92	2.24*	0.94*
H_l[m]	Vallombrosa	*I_4q_p95 + num_max + AVG_homogeneity + AVG_dissimilarity*	3.3	13.53	0.70	0.95	2.26*	0.93*
	Rincine	*AVG_entropy + SD_entropy + p7 + AVG_contrast*	4.0	15.06	0.60	1.04	1.39*	0.89*
H_{σ}[m]	Vallombrosa	i2q_d10 + min_B + num_max + AVG_homogeneity	1.13	15.93	0.64	0.94	2.62*	0.87*
	Rincine	SD_homogeneity + p7	0.52	16.92	0.65	0.95	2.98*	0.86*
V[m^3ha^{-1}]	Vallombrosa	I_quant_1 + i_1q_d5 + num_max + AVG_homogeneity	96.1	15.95	0.79	0.91	3.25*	0.84*
	Rincine	I_1q_p5	122.2	24.34	0.78	0.92	3.57*	0.87*

[a] see Annex 1 for a complete description of the variables.

(15.06% ≤ $RMSE_{\%}$ ≤ 29.00%) (Fig. 3).

In both the areas DTM-independent models produced accurate results in modelling the V (Table 3 and Fig. 3), even if the models based on ALS achieved slightly better results (Table 4 and Fig. 3). In Vallombrosa the predictive accuracy of the estimate for V ($RMSE_{\%}$ = 15.95) was slightly higher than in Rincine ($RMSE_{\%}$ = 24.34) most probably because the forest of Vallombrosa is composed by high forests and the volumes in the different forest stands are more homogeneous than in Rincine where there is a greater mixture of coppices and high forests. In terms of $RMSE_{\%}$, the predictive accuracy of DTM-independent models for V in both study areas was comparable to that of previous studies based on ALS variables in similar forests for which $RMSE_{\%}$ typically ranged between 16.7% and 30% (Corona & Fattorini 2008; Barbati et al., 2009; Tonolli et al., 2011; Bottalico et al., 2017; Giannetti et al., 2018a). In Vallombrosa we found comparable results with the ones obtained by Jayathunga et al. (2018) in an uneven-aged mixed conifer-broadleaf forest (i.e. $RMSE_{\%}$ = 16.7%) and the ones of Puliti et al. (2015) in one boreal forest (i.e. $RMSE_{\%}$ = 14.95%) using height metrics calculated on normalized photogrammetric point cloud with DTM based on ALS, while Shen et al. (2019), in less complex forest i.e. ginkgo plantation in China, reached lower $RMSE_{\%}$ for V (i.e. between 13.26% and 14.33%) using height

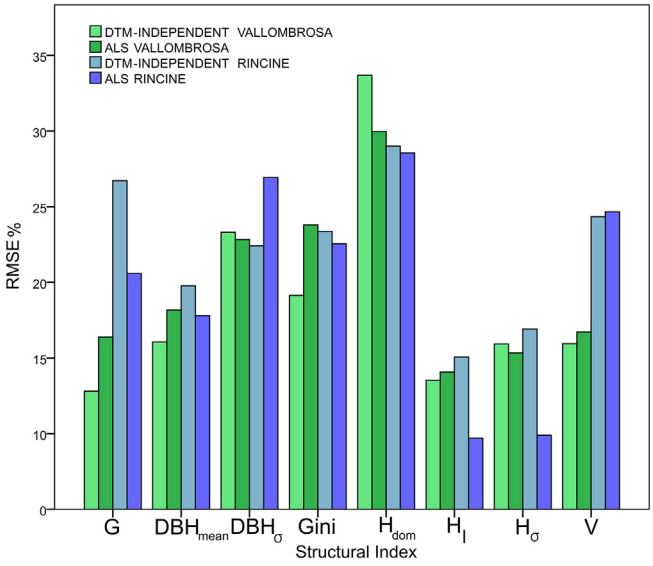

Fig. 2. Bar plots of $RMSE_{\%}$ for the two different study areas, for each of the forest structure indices, and the different sets of variables.

Table 4
Variables selections and models accuracies, in terms of RMSE, $RMSE_{\%}$, Adj.R^2, SRR and Hypothesis test for the multiple regression models using the ALS variables as predictors (α = intercept slope of observed vs predicted regression; β = slope of observed vs prediction regression; level of significance for rejection [*not significant < 0.001]).

Structural index	Study Area	ALS variables	RMSE	$RMSE_{\%}$	Adj. R^2	SSR	HT α	HT β
G [m^2ha^{-1}]	Vallombrosa	*p10*	9.40	16.39	0.54	0.96	1.56*	0.90*
	Rincine	*d7 + d8 + d9 + CV*	9.84	20.58	0.69	0.97	1.42*	0.83*
DBH_{mean} [cm]	Vallombrosa	*p99*	5.01	18.18	0.39	0.95	2.10*	0.91*
	Rincine	*p9 + all*	4.84	17.80	0.72	0.91	2.41*	0.93*
DBH_{σ} [cm]	Vallombrosa	*std + kur + b30 + b80*	2.76	22.83	0.61	0.89	2.54*	0.89*
	Rincine	*p9 + d1 + CV + AAD*	2.03	26.93	0.42	0.92	2.25*	0.93*
Gini [0,1]	Vallombrosa	*d2*	0.11	23.79	0.25	0.95	1.19*	0.95*
	Rincine	*d1 + d6 + CV*	0.073	22.55	0.71	0.97	2.21*	0.91*
H_{dom} [m]	Vallombrosa	*p10 + d6*	2.13	29.97	0.56	0.92	1.21*	0.96*
	Rincine	*d3 + d2 + d1 + CV*	1.04	28.56	0.33	0.94	1.44*	0.97*
H_l [m]	Vallombrosa	*p75*	3.49	14.08	0.71	0.91	2.34*	0.94*
	Rincine	*p95*	2.44	9.71	0.87	0.98	1.25*	0.92*
H_{σ} [m]	Vallombrosa	*p75*	1.08	15.34	0.73	0.97	1.34*	0.86*
	Rincine	*p95*	0.30	9.90	0.91	0.91	1.26*	0.92*
V [m3ha^{-1}]	Vallombrosa	*p75*	100.81	16.72	0.79	0.89	2.46*	0.94*
	Rincine	*p75*	122.29	24.66	0.76	0.92	1.69*	0.92*

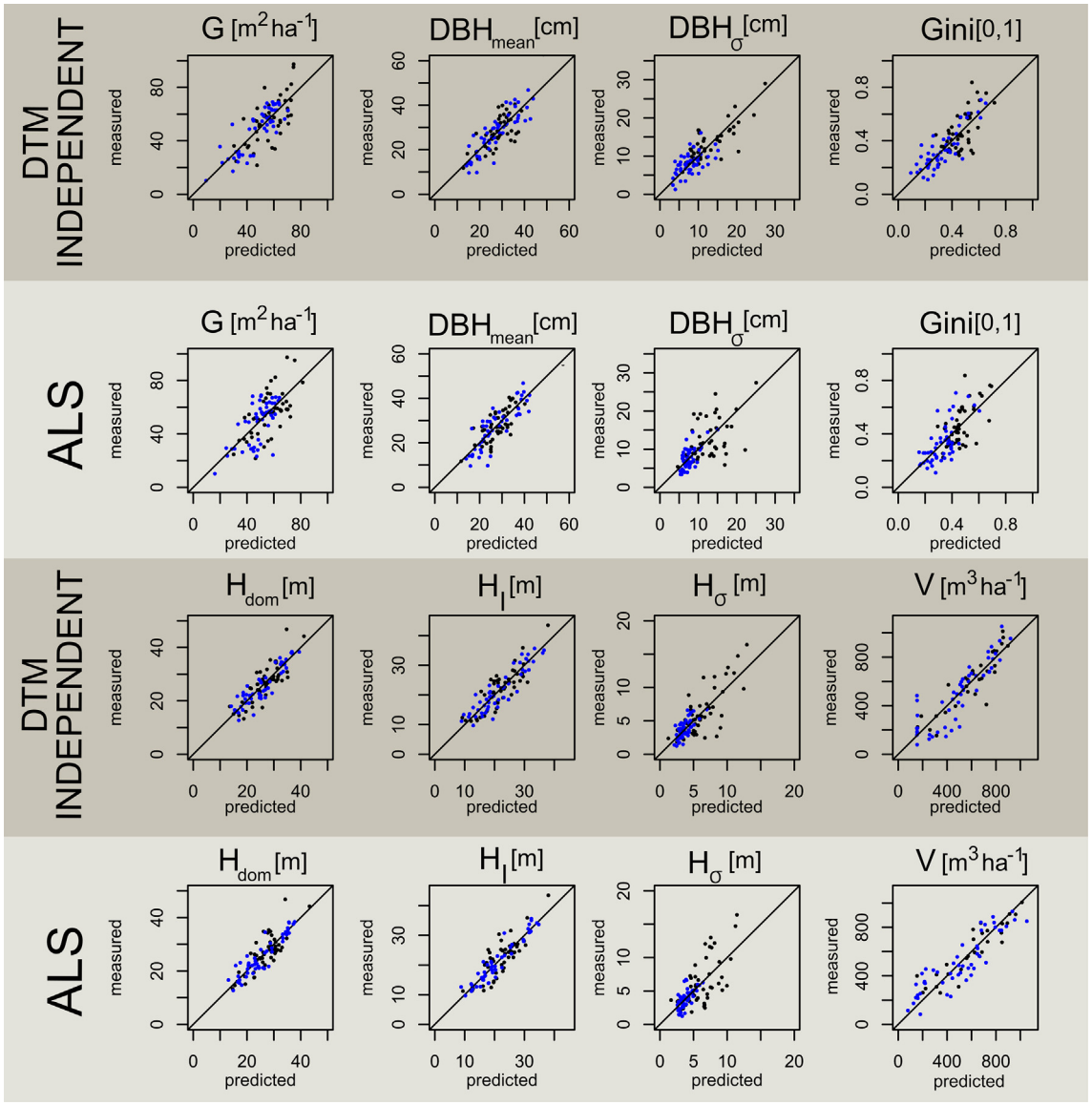

Fig. 3. Scatterplot of measured versus predicted values for the models using UAV DTM-independent variables (dark gray background) and ALS variables (light grey background). Black dots represent Vallombrosa while blue dots are for Rincine.

metrics and spectral variables derived by UAV hyperspectral photogrammetry data. Among the two types of forests, DTM-independent models produced more accurate results in terms of $RMSE_{\%}$ and *Adj.* R^2 for G, DBH_{mean}, Gini, and H_{dom} in Vallombrosa and for σ_{dbh} in Rincine compared to the ones obtained by ALS. Moreover, the accuracy obtained in the current study using DTM-independent models, in both study areas, was larger or comparable for G, DBH_{mean} DBH_{σ}, H_{σ}, and H_{dom} with those obtained with ALS variables by Bottalico et al. (2017) in a Mediterranean forest and those obtained by Mura et al. (2015) in a temperate forest. For Gini structure indices, the accuracy of DTM-independent models in terms of $RMSE_{\%}$ (Table 3) is consistent with the ones obtained by Valbuena et al. (2016), with ALS variables (Table 4), in two boreal forests: one unmanaged for conservation purposes (i.e. $RMSE_{\%}$ = 20.24%) and one used for maximizing commercial economic returns (i.e. $RMSE_{\%}$ = 18.78%). However, we found lower RMSE% in unmanaged forest (i.e. Vallombrosa) respect to the one that we obtained in managed forest (i.e. Rincine) while Valbuena et al. (2016) reported the opposite. Moreover, we found that the Gini DTM-independent model in Vallombrosa produced an $RMSE_{\%}$ that is 4.65% points lower than those obtained by the ALS model, while comparable results between DTM-independent and ALS models were observed in Rincine. For the indices related to tree height (i.e. H_{dom}, H_l, and σ_h), ALS produced always better results compared to those obtained by DTM-independent models. These results were expected because normalized ALS metrics are directly related with the canopy height.

Concerning the uncertainty of the estimates, the use of remotely sensed data consistently increased the precision of the design-based estimates meaning that the DTM-independent approach can reduce the costs of field surveys while providing detailed spatially explicit information of forest biodiversity (Saarinen et al., 2018). We found that even though ALS-based estimates were, on average, more efficient (average RE ALS = 3.7) than the ones from DTM-independent variables (average RE DTM-independent = 3.3), the latter resulted consistently in larger RE than ALS for G, DBH_{mean}, DBH_{σ}, and V. These findings were in contrast with what previously shown by Puliti et al. (2020), who within a model-based framework and using DTM-independent variables, found relative efficiencies limited to 1 and 1.1 when estimating G and V. Since Puliti et al. (2020) adopted different inferential framework (i.e., model-based), a further explanation of such discrepancy could be that in our experiment the study areas were larger (115 and 290 ha) and more diverse than the 40 ha monospecific stand in Puliti et al. (2020). These two were limiting factors in Puliti et al. (2020), which

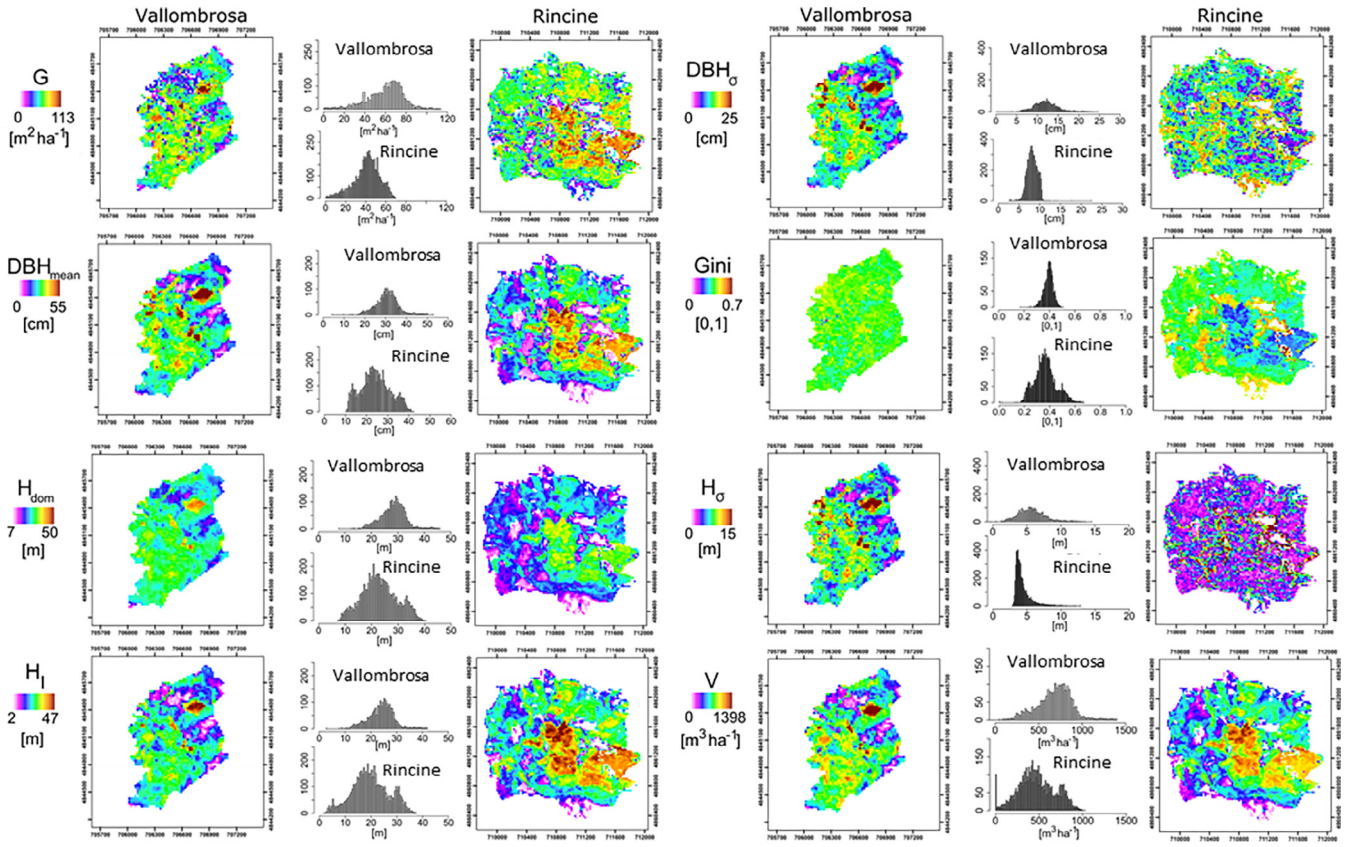

Fig. 4. Maps and histograms of the eight structure indices obtained by applying the models based on UAV DTM-independent variables for the two study areas.

affected the spatial autocorrelation in their models, which can be considered negligible for large areas (McRoberts et al., 2018). Based on the RE for the DTM-independent predictors, it is possible to calculate the number of field plots required to obtain the same level of precision as for the model-assisted DTM-independent predictors but using only field plot data. On average, for Vallombrosa and for Rincine two and six times (see Table 5) the number of plots would have been required to obtain the same level of precision as for DTM-independent model-assisted estimates. This highlights the potential of DTM-independent variables, which not only can be used virtually on any forests (i.e., no need of a DTM) but also can produce as precise estimates as ALS data for key forest structural variables and substantially improve the efficiency of forest inventories.

We found that the DTM-independent models produced consistent results in monitoring forest structure variables across two different types of management systems also if the variations in forest management lead to some differences in the structural properties of forests (Lilja and Kuuluvainen, 2005; Uuttera et al., 1998).

Consistently with the findings by Giannetti et al. (2018a) and Puliti et al. (2019) this study confirmed that DTM-independent variables are

Table 5
Estimators of mean and variance according to the GREG estimator for the mean value of the forest structural indices, the standard error (SE) of the two areas obtained using the model-assisted regression (Särndal et al. 2003) using DTM-independent models and ALS models. The relative efficiency (RE) was calculated as the ratio between the variance of design-based estimates and the variance of model-assisted regression of DTM-independent models and of ALS models.

	DTM-independent $\hat{\mu}_{GREG}$	DTM-independent $SE(\hat{\mu}_{GREG})$	RE DTM-independent	ALS $\hat{\mu}_{GREG}$	ALS $SE(\hat{\mu}_{GREG})$	RE ALS
Vallombrosa						
G [m^2ha^{-1}]	58.28	3.21	1.6	58.76	3.32	1.6
DBH_{mean} [cm]	30.7	0.013	2.2	30.7	0.014	1.93
DBH_{σ} [cm]	12.03	0.51	2.3	12.2	0.52	2.1
Gini [0,1]	0.39	0.02	1.07	0.38	0.02	1.07
H_{dom} [m]	28.13	0.93	2.8	28.34	0.89	3.12
H_l [m]	23.94	0.79	3.68	24.3	0.70	4.7
H_{σ} [m]	5.70	0.53	2.3	5.6	0.48	2.8
V [m^3ha^{-1}]	683.22	18.73	5.1	693.4	19.21	4.85
Rincine						
G [m^2ha^{-1}]	42.31	1.27	3.44	43.24	1.45	2.64
DBH_{mean} [cm]	25.62	0.65	4.2	26.2	0.46	3.92
DBH_{σ} [cm]	7.54	0.28	2.02	7.45	0.32	1.55
Gini [0,1]	0.37	0.0.1	4.21	0.36	0.01	4.54
H_{dom} [m]	23.62	0.41	6.02	23.7	0.35	8.1
H_l [m]	19.91	0.41	6.43	19.82	0.30	11.7
H_{σ} [m]	3.62	0.17	1.3	3.66	0.14	1.8
V [m^3ha^{-1}]	483.22	17.65	4.2	485.22	18.9	3.7

viable predictors for forest structure indices. The DTM-independent models were also useful to create maps of forest structure indices that can be used for forest management purposes and to estimate area population means using GREG estimators (Baffetta et al., 2009; Bottalico et al., 2017; Chirici et al., 2020; McRoberts et al., 2013; Mura et al., 2015) that can be used independently of the modelling approach used for estimated bias resulting from systematic deviations between observations and predictions. Several authors underlined the importance of forest structure indices for forest biodiversity monitoring (Valbuena et al. 2016, Corona et al. 2017; Mura et al., 2015). Wall-to-wall maps of forest structural indices are useful to make better decisions in support sustainable forest management, and forest certification. It is important to remember that while at the pixel level, these maps may be affected by a substantial bias, when aggregating several pixels values to areas of increasing size (e.g., forest stand, forest property) the average value tends to equal real value if we assume the residuals to be independent and with zero mean (McRoberts and Tomppo, 2007). Moreover, these maps can be used to support planning for small area monitoring and management interventions that would not be feasible using ground data only and could be the basis for decision support systems as proposed by Puletti et al. (2017). Decision Support Systems can be useful to assess, for example, wood production, harvesting activities, and to quantify ecosystems services usefyl to support and to develop forest management plans (Bottalico et al., 2016; Vizzarri et al., 2017). Moreover, the wall-to-wall maps of structural diversity can be used not only for planning management strategies addressing biodiversity (Winter et al., 2018), but also for timber production purposes, as tree diameters and heights are basic information for assessing the commercial value of tree logs (Arvola et al., 2019; Vacchiano et al., 2018).

Our results show that these maps can be useful in comparing different forests and thus to provide suitable data to support more adaptive management strategies. When comparing the maps of DBH_{σ}, and H_{σ} indices across the two study areas (Fig. 4), it is possible to note that the variability in the vertical and horizontal stratum is larger in Vallombrosa than in Rincine. These results were somewhat expected because of the different forest management regimes adopted in the two study areas with the Vallombrosa characterized by a more diverse forest structure than Rincine, which is actively managed for timber production. As reported by Lexerød and Eid, (2006) if tree size diversity is small, almost all trees became mature for productive purposes at the same time, while large tree size diversity ensures a wide range of habitats providing a high level of biodiversity. Future investigations should focus on the transferability of the approach we developed over larger areas and in the framework of the activities routinely carried out in National Forest Inventories, for example, to understand if specific models need to be developed to take into account different species composition and management regimes.

5. Conclusion

This research denibstrated that UAV 3D photogrammetric data alone (i.e., without the need of a digital terrain model) are suitable for modeling, mapping, and estimating forest structure indices in mixed temperate forests with similar or better accuracy than those obtained with ALS data. In this study, in addition to assessing the model's performances (e.g., model fit and predictive accuracy), we adopted a statistically rigorous approach to estimating the mean values for each variable of interest and its uncertainty within a model-assisted inferential framework (i.e., GREG estimator). We found a substantial boost in the precision of the estimates based on DTM-independent variables over the use of field data alone in a design-based framework. Future research efforts should focus on extending the results for estimating different forest biodiversity-related variables (e.g., deadwood) and to test the proposed methodology in different forest types (e.g., tropical, alpine, Mediterranean, boreal) in order to evaluate if DTM-independent approach can potentially increase the area of application of UAV photogrammetry over different parts of the globe. Moreover, future studies should address the transferability of the model to new areas where no field plots are available.

Authors contributions

Francesca Giannetti designed the experiment, carrued out UAV data acquisition, data processing, statistical analysis, and wrote the first draft manuscript. Davide Travaglini and Gherardo Chirici designed the field sampling schemes. Stefano Puliti, Nicola Puletti, Gherardo Chirici and Davide Travaglini co-authored and revised the manuscript.

Acknowledgments

This research was supported by the LIFE programme in the framework of the project "FRESh LIFE—Demonstrating Remote Sensing integration in sustainable forest management" (LIFE14 ENV/IT/000414) and in part by Accademia Italiana di Scienze Forestali in the framework of PhD Student Scholarship given to Francesca Giannetti.

We wish to thank Andrea Barzagli, Barbara Del Perugia, Marta Galluzzi, and Duccio Bacci for the field work in Rincine District and all the graduating students of the University of Florence for their help in fieldwork data acquisition in the Vallombrosa forest. We wish to thank also Tony Ventre for his supporting UAV data acquisition in Rincine District during the field campain. We are grateful to three anonymous reviewers and the Editor who contributed to improving the original version of the manuscript with their suggestions and comments.

Appendix A. Supplementary data

Supplementary data to this article can be found online at https://doi.org/10.1016/j.ecolind.2020.106513.

References

Adhikari, H., Valbuena, R., Pellikka, P.K.E., Heiskanen, J., 2020. Mapping forest structural heterogeneity of tropical montane forest remnants from airborne laser scanning and Landsat time series. Ecol. Indic. 108, 105739. https://doi.org/10.1016/j.ecolind.2019.105739.

Agisoft LLC, 2017. Agisoft PhotoScan User Manual. Available online http://www.agisoft.com/pdf/photoscan-pro_1_3_en.pdf (accessed on 11 April 2017).

Arabatzis, G., 2010. Development of Greek forestry in the framework of the European Union policies. J. Environ. Prot. Ecol. 11, 682–692.

Arvola, A., Malkamäki, A., Penttilä, J., Toppinen, A., 2019. Mapping the future market potential of timber from small-scale tree farmers: perspectives from the Southern Highlands in Tanzania. Small-scale For. 18, 189–212. https://doi.org/10.1007/s11842-019-09414-8.

Baffetta, F., Fattorini, L., Franceschi, S., Corona, P., 2009. Design-based approach to k-nearest neighbours technique for coupling field and remotely sensed data in forest surveys. Remote Sens. Environ. 113, 463–475. https://doi.org/10.1016/j.rse.2008.06.014.

Bagaram, M.B., Giuliarelli, D., Chirici, G., Giannetti, F., Barbati, A., 2018. UAV remote sensing for biodiversity monitoring: are forest canopy gaps good covariates ? Remote Sens. 1–29. https://doi.org/10.3390/rs10091397.

Barabesi, L., Franceschi, S., 2011. Sampling properties of spatial total estimators under tessellation stratified designs. Environmetrics 22, 271–278. https://doi.org/10.1002/env.1046.

Barabesi, L., Franceschi, S., Marcheselli, M., 2012. Stratified spatial sampling with application to canopy coverage estimation. Ann. Appl. Stat. 6, 210–228. https://doi.org/10.1214/11-AOAS509.

Barbati, A., Chirici, G., Corona, P., Montaghi, A., Travaglini, D., 2009. Area-based assessment of forest standing volume by field measurements and airborne laser scanner data. Int. J. Remote Sens. 30, 5177–5194. https://doi.org/10.1080/01431160903023017.

Barbati, A., Marchetti, M., Chirici, G., Corona, P., 2014. European Forest Types and Forest Europe SFM indicators: tools for monitoring progress on forest biodiversity conservation. For. Ecol. Manage. 321, 145–157. https://doi.org/10.1016/j.foreco.2013.07.004.

Batisteli, A.F., Tanaka, M.O., Souza, A.L.T., 2018. Bird functional traits respond to forest structure in riparian areas undergoing active restoration. Diversity 10, 8–11. https://doi.org/10.3390/d10030090.

Beedy, E.C., 1981. Bird communities and forest structure in the sierra Nevada of California. Condor 83, 97–105.

Bergner, A., Avcı, M., Eryiğit, H., Jansson, N., Niklasson, M., Westerberg, L., Milberg, P., 2015. Influences of forest type and habitat structure on bird assemblages of oak

(Quercus spp.) and pine (Pinus spp.) stands in southwestern Turkey. For. Ecol. Manage. 336, 137–147. https://doi.org/10.1016/j.foreco.2014.10.025.
Bohlin, J., Wallerman, J., Fransson, J.E.S., 2012. Forest variable estimation using photogrammetric matching of digital aerial images in combination with a high-resolution DEM. Scand. J. For. Res. 27, 692–699. https://doi.org/10.1080/02827581.2012.686625.
Bottalico, F., Chirici, G., Giannini, R., Mele, S., Mura, M., Puxeddu, M., McRoberts, R.E., Valbuena, R., Travaglini, D., 2017. Modeling Mediterranean forest structure using airborne laser scanning data. Int. J. Appl. Earth Obs. Geoinf. 57, 145–153. https://doi.org/10.1016/j.jag.2016.12.013.
Bottalico, F., Persola, L., Vizzarri, M., Antonello, L., Barbati, A., Chirici, G., Corona, P., Cullotta, S., Garfì, V., Giannico, V., Lafortezza, R., Lombardi, F., Marchetti, M., Nocentini, S., Riccioli, F., Travaglini, D., Sallustio, L., 2016. Modeling the influence of alternative forest management scenarios on wood production and carbon storage: A case study in the Mediterranean region. Environ. Res. 144, 72–87. https://doi.org/10.1016/j.envres.2015.10.025.
Bottalico, F., Travaglini, D., Fiorentini, S., Lisa, C., Nocentini, S., 2014. Stand dynamics and natural regeneration in silver fir (Abies alba Mill.) plantations after traditional rotation age. iForest – Biogeosci. For. 7, 313–323. https://doi.org/10.3832/ifor0985-007.
Bradshaw, R.H.., Lindén, M., 1997. RENFOR. Regeneration of natural forest stand for timber production and environmental value.
Brosofske, K.D., Froese, R.E., Falkowski, M.J., Banskota, A., 2014. A review of methods for mapping and prediction of inventory attributes for operational forest management. For. Sci. 60, 733–756. https://doi.org/10.5849/forsci.12-134.
Bruniquel-Pinel, V., Gastellu-Etchegorry, J.P., 1998. Sensitivity of texture of high resolution images of forest to biophysical and acquisition parameters. Remote Sens. Environ. 65, 61–85. https://doi.org/10.1016/S0034-4257(98)00009-1.
Chirici, G., Bottalico, F., Giannetti, F., Del Perugia, B., Travaglini, D., Nocentini, S., Kutchartt, E., Marchi, E., Foderi, C., Fioravanti, M., Fattorini, L., Bottai, L., McRoberts, R.E.R.E., Næsset, E., Corona, P., Gozzini, B., Del Perugia, Barbara, Travaglini, D., Nocentini, S., Kutchartt, E., Marchi, E., Foderi, C., Fioravanti, M., Fattorini, L., Bottai, L., McRoberts, R.E.R.E., Naesset, E., Corona, P., Gozzini, B., 2018. Assessing forest windthrow damage using single-date, post-event airborne laser scanning data. For. An Int. J. For. Res. 1, 27–37. https://doi.org/10.1093/forestry/cpx029.
Chirici, G., Giannetti, F., McRoberts, R.E., Travaglini, D., Pecchi, M., Maselli, F., Chiesi, M., Corona, P., 2020. Wall-to-wall spatial prediction of growing stock volume based on Italian National Forest Inventory plots and remotely sensed data. Int. J. Appl. Earth Obs. Geoinf. 84, 101959. https://doi.org/10.1016/j.jag.2019.101959.
Chirici, G., McRoberts, R.E., Winter, S., Bertini, R., Bröändli, U.-B., Asensio, I.A., Bastrup-Birk, A., Rondeux, J., Barsoum, N., Marchetti, M., 2012. National forest inventory contributions to forest biodiversity monitoring. For. Sci. 58, 257–268. https://doi.org/10.5849/forsci.12-003.
Clausen, J., Perregaard, M., 1999. On the best search strategy in parallel branch-and-bound: Best-First Search versus Lazy Depth-First Search. Ann. Oper. Res. 90, 1–17. https://doi.org/10.1023/A:1018952429396.
Corona, P., 2010. Integration of forest mapping and inventory to support forest management. IForest 3, 59–64. https://doi.org/10.3832/ifor0531-003.
Corona, P., Chianucci, F., Quatrini, V., Civitarese, V., Clementel, F., Costa, C., Floris, A., Menesatti, P., Puletti, N., Sperandio, G., Verani, S., Turco, R., Bernardini, V., Plutino, M., Scrinzi, G., 2017. Precision forestry: concepts, tools and perspectives in Italy. For. – Riv. di Selvic. ed Ecol. For. 14, 1–12. https://doi.org/10.3832/efor2285-014.
Corona, P., Chirici, G., McRoberts, R.E., Winter, S., Barbati, A., 2011. Contribution of large-scale forest inventories to biodiversity assessment and monitoring. For. Ecol. Manage. 262, 2061–2069. https://doi.org/10.1016/j.foreco.2011.08.044.
Corona, P., Fattorini, L., 2008. Area-based lidar-assisted estimation of forest standing volume. Can. J. For. Res. 38, 2911–2916. https://doi.org/10.1139/X08-122.
Davies, O.L., Goldsmith, P.L., 1984. Statistical methods in research and production : with special reference to the Chemical Industry, Longman. ed. London.
Esseen, P.-A., Ehnström, B., Ericson, L., Sjöberg, K., 1992. Boreal Forests—The Focal Habitats of Fennoscandia. In: Hansson, L. (Ed.), Ecological Principles of Nature Conservation: Application in Temperate and Boreal Environments. Springer, US, Boston, MA, pp. 252–325. https://doi.org/10.1007/978-1-4615-3524-9_7.
European Commission, 2013. A new EU Forest Strategy: for forests and the forest-based sector. Commun. from Comm. to Counc. Eur. Parliam. Eur. Econ. Soc. Comm. Comm. Reg. 17. https://doi.org/10.1017/CBO9781107415324.004.
European Environment Agency, 2012. Streamlining European biodiversity indicators 2020: Building a future on lessons learnt from the SEBI 2010 process. Copenhagen.
Evans, J.S., Hudak, A.T., Faux, R., Smith, A.M.S., 2009. Discrete return lidar in natural resources: recommendations for project planning, data processing, and deliverables. Remote Sens. 1, 776–794. https://doi.org/10.3390/rs1040776.
Fardusi, M.J., Chianucci, F., Barbati, A., 2017. Concept to Practices of Geospatial Information Tools to Assist Forest Management and Planning under Precision Forestry Framework : a review 41, 3–14.
Fattorini, L., Puletti, N., Chirici, G., Corona, P., Gazzarri, C., Mura, M., Marchetti, M., 2016. Checking the performance of point and plot sampling on aerial photoimagery of a large-scale population of trees outside forests. Can. J. For. Res. 46, 1264–1274. https://doi.org/10.1139/cjfr-2016-0013.
Forest Europe, 2015. State of Europe's Forests 2015. Ministerial Conference on the Protection of Forests in Europe, FOREST EUROPE Liaison Unit Madrid.
Fotakis, D.G., Sidiropoulos, E., Myronidis, D., Ioannou, K., 2012. Spatial genetic algorithm for multi-objective forest planning. For. Policy Econ. 21, 12–19. https://doi.org/10.1016/j.forpol.2012.04.002.
Franklin, J.F., DeBell, D.S., 1988. Thirty-six years of tree population change in an old-growth Pseudotsuga-Tsuga forest. Can. J. For. Res. 18, 633–639. https://doi.org/10.1139/x88-093.
Galluzzi, M., Giannetti, F., Puletti, N., Canullo, R., Rocchini, D., Bastrup, A., Gherardo, B., 2019. A plot – level exploratory analysis of European forest based on the results from the BioSoil Forest Biodiversity project. Eur .J. For. Res. https://doi.org/10.1007/s10342-019-01205-2.
Giannetti, F., Barbati, A., Mancini, L.L.D., Travaglini, D., Bastrup-Birk, A., Canullo, R., Nocentini, S., Chirici, G., 2017. European Forest types: toward an automated classification. Ann. For. Sci. 99. https://doi.org/10.1007/s13595-017-0674-6.
Giannetti, F., Chirici, G., Gobakken, T., Næsset, E., Travaglini, D., Puliti, S., 2018a. A new approach with DTM-independent metrics for forest growing stock prediction using UAV photogrammetric data. Remote Sens. Environ. 213. https://doi.org/10.1016/j.rse.2018.05.016.
Giannetti, Francesca, Chirici, G., Gobakken, T., Næsset, E., Travaglini, D., Puliti, S., 2018b. A new approach with DTM-independent metrics for forest growing stock prediction using UAV photogrammetric data. Remote Sens. Environ. 213, 195–205. https://doi.org/10.1016/j.rse.2018.05.016.
Gómez, C., Wulder, M.A., Montes, F., Delgado, J.A., 2012. Forest structural diversity characterization in Mediterranean pines of central Spain with QuickBird-2 imagery and canonical correlation analysis. Can. J. Remote Sens. 37, 628–642. https://doi.org/10.5589/m12-005.
Hanle, J., Duguid, M.C., Ashton, M.S., 2020. Legacy forest structure increases bird diversity and abundance in aging young forests. Ecol. Evol. 1193–1208. https://doi.org/10.1002/ece3.5967.
Haralick, R.M., Shanmugam, K., Dinstein, I., 1973. Textural Features for Image Classification.
Hese, S., Behrendt, F., 2017. Multiseasonal tree crown structure mapping with point clouds from OTS quadrocopter systems. Int. Arch. Photogramm. Remote Sens. Spat. Inf. Sci. – ISPRS Arch. 42, 141–143. https://doi.org/10.5194/isprs-archives-XLII-2-W6-141-2017.
Iglhaut, J., Cabo, C., Puliti, S., Piermattei, L., O'Connor, J., Rosette, J., Connor, J.O., Rosette, J., Connor, J.O., 2019. Structure from motion photogrammetry in forestry: a review. Curr. For. Reports. https://doi.org/10.1007/s40725-019-00094-3.
Immitzer, M., Stepper, C., Böck, S., Straub, C., Atzberger, C., 2016. Forest Ecology and Management Use of WorldView-2 stereo imagery and National Forest Inventory data for wall-to-wall mapping of growing stock. For. Ecol. Manage. 359, 232–246. https://doi.org/10.1016/j.foreco.2015.10.018.
International Model Forest Network (IMFN), 2008. Guide to Model Forest Governance.
Isenburg, M., 2017. LAStools – efficient LiDAR processing software, obtained from http://rapidlasso.com/LAStools.
Jayathunga, S., Owari, T., Tsuyuki, S., 2018. The use of fixed–wing UAV photogrammetry with LiDAR DTM to estimate merchantable volume and carbon stock in living biomass over a mixed conifer–broadleaf forest. Int. J. Appl. Earth Obs. Geoinf. 73, 767–777. https://doi.org/10.1016/j.jag.2018.08.017.
Kachamba, D., Ørka, H., Gobakken, T., Eid, T., Mwase, W., 2016. Biomass estimation using 3D data from unmanned aerial vehicle imagery in a tropical woodland. Remote Sens. 2016 (8), 968. https://doi.org/10.3390/RS8110968.
Kolb, T.E., Wagner, M.R., Covington, W.W., 1994. Concepts of forest entomology. J. For. 9, 337–338. https://doi.org/10.1093/forestscience/9.3.337.
Kurttila, M., 2001. The spatial structure of forests in the optimization calculations of forest planning – a landscape ecological perspective. For. Ecol. Manage. 142, 129–142. https://doi.org/10.1016/S0378-1127(00)00343-1.
Lefsky, M., Cohen, W.B., Parker, G.G., Harding, D.J., 2002. Lidar remote sensing for ecosystem studies. Bioscience 52, 19–30. https://doi.org/10.1641/0006-3568(2002)052[0019:LRSFES]2.0.CO;2.
Lexerød, N.L., Eid, T., 2006. An evaluation of different diameter diversity indices based on criteria related to forest management planning. For. Ecol. Manage. 222, 17–28. https://doi.org/10.1016/j.foreco.2005.10.046.
Lilja, S., Kuuluvainen, T., 2005. Structure of old Pinus sylvestris dominated forest stands along a geographic and human impact gradient in mid-boreal Fennoscandia. Silva Fenn. 39, 407–428. https://doi.org/10.14214/sf.377.
Lim, K.P., Treitz, P., Wulder, M.A., St-Onge, B.A., Flood, M., 2003. LiDAR remote sensing of forest structure. Prog. Phys. Geogr. 27, 88–106.
Lindberg, E., Roberge, J.M., Johansson, T., Hjältén, J., 2015. Can airborne laser scanning (ALS) and forest estimates derived from satellite images be used to predict abundance and species richness of birds and beetles in boreal forest? Remote Sens. 7, 4233–4252. https://doi.org/10.3390/rs70404233.
Lisein, J., Pierrot-Deseilligny, M., Bonnet, S., Lejeune, P., 2013. A photogrammetric workflow for the creation of a forest canopy height model from small unmanned aerial system imagery. Forests 4, 922–944. https://doi.org/10.3390/f4040922.
Lumley, T., 2017. Package "leaps": Regression Subset Selection vs. 3.0 8.
Marra, E., Cambi, M., Fernandez-Lacruz, R., Giannetti, F., Marchi, E., Nordfjell, T., 2018. Photogrammetric estimation of wheel rut dimensions and soil compaction after increasing numbers of forwarder passes. Scand. J. For. Res. https://doi.org/10.1080/02827581.2018.1427789.
McElhinny, C., Gibbons, P., Brack, C., Bauhus, J., 2005. Forest and woodland stand structural complexity: Its definition and measurement. For. Ecol. Manage. 218, 1–24. https://doi.org/10.1016/j.foreco.2005.08.034.
McGaughey, R.J., 2014. FUSION/LDV: Software for LIDAR Data Analysis and Visualization 154.
McRoberts, R.E., Næsset, E., Gobakken, T., 2013. Inference for lidar-assisted estimation of forest growing stock volume. Remote Sens. Environ. 128, 268–275. https://doi.org/10.1016/j.rse.2012.10.007.
McRoberts, R.E., Næsset, E., Gobakken, T., Chirici, G., Condés, S., Hou, Z., Saarela, S., Chen, Q., Ståhl, G., Walters, B.F., 2018. Assessing components of the model-based mean square error estimator for remote sensing assisted forest applications. Can. J. For. Res. 48, 642–649. https://doi.org/10.1139/cjfr-2017-0396.

McRoberts, R.E., Tomppo, E.O., 2007. Remote sensing support for national forest inventories. Remote Sens. Environ. 110, 412–419. https://doi.org/10.1016/j.rse.2006.09.034.
Meng, J., Li, S., Wang, W., Liu, Q., Xie, S., Ma, W., 2016. Estimation of forest structural diversity using the spectral and textural information derived from SPOT-5 satellite images. Remote Sens. 8. https://doi.org/10.3390/rs8020125.
Moser, P., Vibrans, A.C., McRoberts, R.E., Næsset, E., Gobakken, T., Chirici, G., Mura, M., Marchetti, M., 2017. Methods for variable selection in LiDAR-assisted forest inventories. Forestry 90, 112–124. https://doi.org/10.1093/forestry/cpw041.
Mura, M., McRoberts, R.E., Chirici, G., Marchetti, M., 2016. Statistical inference for forest structural diversity indices using airborne laser scanning data and the k-Nearest Neighbors technique. Remote Sens. Environ. 186, 678–686. https://doi.org/10.1016/j.rse.2016.09.010.
Mura, M., McRoberts, R.E., Chirici, G., Marchetti, M., 2015. Estimating and mapping forest structural diversity using airborne laser scanning data. Remote Sens. Environ. 170, 133–142. https://doi.org/10.1016/j.rse.2015.09.016.
Næsset, E., 2002. Predicting forest stand characteristics with airborne scanning laser using a practical two-stage procedure and field data. Remote Sens. Environ. 80, 88–99. https://doi.org/10.1016/S0034-4257(01)00290-5.
Næsset, E., 2004. Practical large-scale forest stand inventory using small-footprint airborne scanning laser. Scand. J. For. Res. 19, 164–179.
Niemi, M., Vauhkonen, J., 2016. Extracting canopy surface texture from airborne laser scanning data for the supervised and unsupervised prediction of area-based forest characteristics. Remote Sens. 8, 582. https://doi.org/10.3390/rs8070582.
Noss, R.F., 1990. Indicators for monitoring biodiversity: a hierarchical approach. Conserv. Biol. 4, 355–364.
Nowak, M.M., Dziób, K., Bogawski, P., 2019. Unmanned aerial vehicles (UAVs) in environmental biology: a review. Eur. J. Ecol. 4, 56–74. https://doi.org/10.2478/eje-2018-0012.
Ozdemir, I., 2008. Estimating stem volume by tree crown area and tree shadow area extracted from pansharpened Quickbird imagery in open Crimean juniper forests. Int. J. Remote Sens. 29, 5643–5655. https://doi.org/10.1080/01431160802082155.
Ozdemir, I., Donoghue, D.N.M., 2013. Modelling tree size diversity from airborne laser scanning using canopy height models with image texture measures. For. Ecol. Manage. 295, 28–37. https://doi.org/10.1016/j.foreco.2012.12.044.
Ozdemir, I., Karnieli, A., 2011. Predicting forest structural parameters using the image texture derived from worldview-2 multispectral imagery in a dryland forest, Israel. Int. J. Appl. Earth Obs. Geoinf. 13, 701–710. https://doi.org/10.1016/j.jag.2011.05.006.
Piñeiro, G., Perelman, S., Guerschman, J.P., Paruelo, J.M., 2008. How to evaluate models: observed vs. predicted or predicted vs. observed? Ecol. Modell. 216, 316–322. https://doi.org/10.1016/j.ecolmodel.2008.05.006.
Puletti, N., Floris, A., Scrinzi, G., Chianucci, F., Colle, G., Michelini, T., Pedot, N., Penasa, A., Scalercio, S., Corona, P., 2017. CFOR: a spatial decision support system dedicated to forest management in Calabria. For. – Riv. di Selvic. ed Ecol. For. 14, 135–140. https://doi.org/10.3832/efor2363-014.
Puliti, S., Dash, J.P., Watt, M.S., Breidenbach, J., Pearse, G.D., 2020. A comparison of UAV laser scanning, photogrammetry and airborne laser scanning for precision inventory of small-forest properties. For. An Int. J. For. Res. 93, 150–162. https://doi.org/10.1093/forestry/cpz057.
Puliti, S., Olerka, H., Gobakken, T., Næsset, E., 2015. Inventory of small forest areas using an unmanned aerial system. Remote Sens. 7, 9632–9654. https://doi.org/10.3390/rs70809632.
Puliti, S., Solberg, S., Granhus, A., 2019. Use of UAV Photogrammetric Data for Estimation of Biophysical Properties in Forest Stands Under Regeneration. https://doi.org/10.3390/rs11030233.
Roussel, 2020. Package 'lidR.'.
Saarinen, N., Vastaranta, M., Näsi, R., Rosnell, T., Hakala, T., Honkavaara, E., Wulder, M.A., Luoma, V., Tommaselli, A.M.G., Imai, N.N., Ribeiro, E.A.W., Guimarães, R.B., Holopainen, M., Hyyppä, J., 2018. Assessing biodiversity in boreal forests with UAV-based photogrammetric point clouds and hyperspectral imaging. Remote Sens. 10. https://doi.org/10.3390/rs10020338.
Santopuoli, G., Di Cristofaro, M., Kraus, D., Schuck, A., Lasserre, B., Marchetti, M., 2019. Biodiversity conservation and wood production in a Natura 2000 mediterranean forest. A trade-off evaluation focused on the occurrence of microhabitats. IForest 12, 76–84. https://doi.org/10.3832/ifor2617-011.
Särndal, C.-E., Swensson, B., Wretman, J., 2003. Model assisted survey sampling, Springer. ed. Berlin.
Shang, C., Treitz, P., Caspersen, J., Jones, T., 2019. Estimation of forest structural and compositional variables using ALS data and multi-seasonal satellite imagery. Int. J. Appl. Earth Obs. Geoinf. 78, 360–371. https://doi.org/10.1016/j.jag.2018.10.002.
Shen, X., Cao, L., Yang, B., Xu, Z., Wang, G., 2019. Estimation of forest structural attributes using spectral indices and point clouds from UAS-based multispectral and RGB imageries. Remote Sens. 11, 1–24. https://doi.org/10.3390/rs11070800.
Skovsgaard, J.P., Vanclay, J.K., 2008. Forest site productivity: a review of the evolution of dendrometric concepts for even-aged stands. Forestry 81, 13–31. https://doi.org/10.1093/forestry/cpm041.
St-Onge, B.A., Cavayas, F., 1995. Estimating forest stand structure from high resolution imagery using the directional variogram. Int. J. Remote Sens. 16, 1999–2021. https://doi.org/10.1080/01431169508954535.
Tabacchi, G., Di Cosmo, L., Gasparini, P., Morelli, S., 2011. Stima del volume e della fitomassa delle principali specie forestali italiene, Equazioni di previsione, tavole del volume e tavole della fitomassa arborea epigea.
Taylor, S.E., McDonald, T.P., Veal, M.W., Corley, F.W., Grift, T.E., 2002. Precision Forestry: operational tactics for today and tomorrow. 25th Annu. Meet. Counc. For. Eng, 6.
Teobaldelli, M., Cona, F., Saulino, L., Migliozzi, A., D'Urso, G., Langella, G., Manna, P., Saracino, A., 2017. Detection of diversity and stand parameters in Mediterranean forests using leaf-off discrete return LiDAR data. Remote Sens. Environ. 192, 126–138. https://doi.org/10.1016/j.rse.2017.02.008.
Tonolli, S., Dalponte, M., Vescovo, L., Rodeghiero, M., Bruzzone, L., Gianelle, D., 2011. Mapping and modeling forest tree volume using forest inventory and airborne laser scanning. Eur. J. For. Res. 130, 569–577. https://doi.org/10.1007/s10342-010-0445-5.
Trimble, 2017. Trimble RealWorks® 8.0 User Guide.
Uuttera, J., Haara, A., Tokola, T., Maltamo, M., 1998. Determination of the spatial distribution of trees from digital aerial photographs. For. Ecol. Manage. 110, 275–282. https://doi.org/10.1016/S0378-1127(98)00292-8.
Vacchiano, G., Berretti, R., Motta, R., Mondino, E.B., 2018. Assessing the availability of forest biomass for bioenergy by publicly available satellite imagery. IForest 11, 459–468. https://doi.org/10.3832/ifor2655-011.
Valbuena, R., Eerikäinen, K., Packalen, P., Maltamo, M., 2016. Gini coefficient predictions from airborne lidar remote sensing display the effect of management intensity on forest structure. Ecol. Indic. 60, 574–585. https://doi.org/10.1016/j.ecolind.2015.08.001.
Valbuena, R., Hernando, A., Manzanera, J.A., Görgens, E.B., Almeida, D.R.A., Mauro, F., García-Abril, A., Coomes, D.A., 2017. Enhancing of accuracy assessment for forest above-ground biomass estimates obtained from remote sensing via hypothesis testing and overfitting evaluation. Ecol. Modell. 366, 15–26. https://doi.org/10.1016/j.ecolmodel.2017.10.009.
Valbuena, R., Packalen, P., Mehtätalo, L., García-Abril, A., Maltamo, M., 2013. Characterizing forest structural types and shelterwood dynamics from Lorenz-based indicators predicted by airborne laser scanning. Can. J. For. Res. 43, 1063–1074. https://doi.org/10.1139/cjfr-2013-0147.
van Ewijk, K., Treitz, P., Woods, M., Jones, T., Caspersen, J., 2019. Forest site and type variability in ALS-based forest resource inventory attribute predictions over three Ontario forest sites. Forests 10, 1–26. https://doi.org/10.3390/f10030226.
Vihervaara, P., Mononen, L., Auvinen, A.-P., Virkkala, R., Lü, Y., Pippuri, I., Packalen, P., Valbuena, R., Valkama, J., 2015. How to integrate remotely sensed data and biodiversity for ecosystem assessments at landscape scale. Landsc. Ecol. 30, 501–516. https://doi.org/10.1007/s10980-014-0137-5.
Vizzarri, M., Sallustio, L., Travaglini, D., Bottalico, F., Chirici, G., Garfì, V., Lafortezza, R., Veca, D.S.L.M., Lombardi, F., Maetzke, F., Marchetti, M., 2017. The MIMOSE approach to support sustainable forest management planning at regional scale in mediterranean contexts. Sustain. 9. https://doi.org/10.3390/su9020316.
Wallace, L., Lucieer, A., Malenovský, Z., Turner, D., Vopěnka, P., 2016. Assessment of forest structure using two UAV techniques: a comparison of airborne laser scanning and structure from motion (SfM) point clouds. Forests 7, 1–16. https://doi.org/10.3390/f7030062.
Winter, S., Bauer, T., Strauss, P., Kratschmer, S., Paredes, D., Popescu, D., Landa, B., Guzmán, G., Gómez, J.A., Guernion, M., Zaller, J.G., Batáry, P., 2018. Effects of vegetation management intensity on biodiversity and ecosystem services in vineyards: a meta-analysis. J. Appl. Ecol. 55, 2484–2495. https://doi.org/10.1111/1365-2664.13124.
Zahawi, R.A., Dandois, J.P., Holl, K.D., Nadwodny, D., Reid, J.L., Ellis, E.C., 2015. Using lightweight unmanned aerial vehicles to monitor tropical forest recovery. Biol. Conserv. 186, 287–295. https://doi.org/10.1016/j.biocon.2015.03.031.
Zellweger, F., Braunisch, V., Baltensweiler, A., Bollmann, K., 2013. Remotely sensed forest structural complexity predicts multi species occurrence at the landscape scale. For. Ecol. Manage. 307, 303–312. https://doi.org/10.1016/j.foreco.2013.07.023.
Zenner, E.K., 2005. Investigating scale-dependent stand heterogeneity with structure-area-curves. For. Ecol. Manage. 209, 87–100. https://doi.org/10.1016/j.foreco.2005.01.004.
Ziegler, S.S., 2000. A comparison of structural characteristics between old-growth and postfire second-growth hemlock-hardwood forests in Adirondack Park, New York, U.S.A. Glob. Ecol. Biogeogr. 9, 373–389. https://doi.org/10.1046/j.1365-2699.2000.00191.x.
Zimble, D.A., Evans, D.L., Carlson, G.C., Parker, R.C., Grado, S.C., Gerard, P.D., 2003. Characterizing vertical forest structure using small-footprint airborne LiDAR. Remote Sens. Environ. 87, 171–182.
Zvoleff, A., 2015. Package 'Glcm', 1.2. Available online http://cran.r-project.org/web/packages/glcm/glcm.pdf (accessed on 11 April 2017).